RSC Advances

PAPER

View Article Online
View Journal | View Issue

Cite this: *RSC Adv.*, 2022, **12**, 12303

Thermal properties and reliabilities of myristic acid–paraffin wax binary eutectic mixture as a phase change material for solar energy storage

Zhixuan Fan, Yunchao Zhao, * Xuying Liu, Yu Shi and Dahua Jiang

In this work, a myristic acid (MA)–paraffin wax (PW) binary eutectic phase change material (PCM) was prepared by a melt-solution blending method. The eutectic point of the MA–PW binary system was determined to be 62 wt% MA–38 wt% PW using a cooling curve. In addition, the phase transition properties and thermal stability of MA–PW binary eutectic PCM were investigated by differential scanning calorimetry (DSC) and thermogravimetry (TG) analysis. The melting temperature and latent heat as well as starting temperature of decomposition for MA–PW binary eutectic PCM were 41.99 °C, 171.43 J g^{-1} and 137.86 °C, respectively. Besides, analysis of the chemical and crystal structures of MA, PW and MA–PW revealed no chemical reaction between MA and PW to produce a new molecular structure and no change in the crystal structure. Finally, MA–PW binary eutectic PCM still has good thermal properties and chemical stability after 500 cold–hot cycles.

Received 21st December 2021
Accepted 8th April 2022

DOI: 10.1039/d1ra09238c

rsc.li/rsc-advances

1. Introduction

Fossil fuels have been widely used in all aspects of society. However, in recent years, the efficient use of solar energy and preparation of new energy storage materials have become a worldwide issue, due to the insufficient supply of fossil energy in the world.[1–4] Global economic development and population growth will lead to a persistent energy crisis. Solar energy is one of the world's most promising renewable energy sources, but its application is limited by a number of characteristics such as being intermittent and uncontrollable. Fortunately, phase change materials (PCMs) can store latent heat by changing their phase state, and release energy when needed,[5,6] and the combination of solar energy and PCMs creates a latent heat storage system that is well suited to increase solar energy utilization. When the temperature reaches the melting point of the PCMs, PCMs can melt to store heat in the form of latent heat, when the temperature is below the melting point, PCMs can solidify to release latent heat back to the thermal storage layer. It can both reduce the maximum temperature difference of thermal storage system between the day time and night time and increase the heat storage capacity of the solar thermal storage system. Therefore, phase change materials suitable for solar energy field have been widely studied.[7–11]

PCMs include organic, inorganic and organic–inorganic eutectic PCMs. Furthermore, organic PCMs have been classified into: paraffin, fatty acids, alcohols and lipids. Among them, fatty acids are promising PCMs, on account of the following advantages, high heat capacity, very slight or no supercoiling, non-toxic, non-corrosive, excellent thermal and chemical stability, small volume change during phase transformation, appropriate melting temperature range and so on.[12–15] Furthermore, paraffin waxes (PW) are also a kind of prospective PCMs, they have a wide melting range and large latent heat of melting.[16,17] The PW are divided into different varieties with melting points at 2 °C intervals, such as 52, 54, 56, 58 and other grades.[18] However, the high phase transition temperature of pure matter prevents widespread application in certain regions with weak solar radiation and low average temperatures. Fortunately, a series of phase change energy storage materials with different phase transition temperatures can be obtained by compounding two or more organic phase change materials,[19,20] and the eutectic materials with various phase change temperatures can complement each other and produce synergistic effects in terms of performance. Therefore, the continuous development of new eutectic PCM with good performance can broaden the application scenarios of phase change energy storage technology, provide engineers with more diverse options, and stimulate the continuous optimization and development of solar thermal storage technology. Karaipekli *et al.*[21,22] studied a number of fatty acid eutectic mixtures and found that fatty acids are suitable candidates for energy storage. Chinnasamy *et al.*[23] prepared a binary eutectic mixture of 40% lauric acid and 60% myristyl alcohol, and found the mixture has excellent thermal properties and chemical stability. Ma *et al.*[24] prepared stearic acid-*n*-butyramide and stearic acid-*n*-octanamide binary eutectic mixtures melting at 64.25 °C and 63.13 °C with latent heat of 198.38 J g^{-1} and 198.98 J g^{-1}, moreover, they

Jiangxi Province Key Laboratory of Environmental Geotechnical Engineering and Hazards Control, Jiangxi University of Science and Technology, Ganzhou 341000, Jiangxi Province, China. E-mail: 465654315@qq.com

believed that the mixtures have good thermal performance and great utility for solar heat storage.

However, reports about eutectic mixtures of fatty acids and PW are very rare so far. The research on these mixtures is very significant and beneficial for development of PCM. Therefore, in this paper, firstly, a fatty acid–paraffin binary eutectic phase change material compounded by myristic acid (MA) and PW was prepared. Secondly, the thermophysical properties of MA, PW and their mixtures were measured by differential scanning calorimetry (DSC), step cold test and thermogravimetry (TG) analysis. Furthermore, the chemical properties of MA, PW and their eutectic mixtures were characterized by X-ray diffraction (XRD) and Fourier Transform Infrared spectroscopic (FT-IR). At last, after accelerated thermal cycling test of eutectic PCM, its thermal and chemical reliability were investigated by using DSC and FT-IR.

2. Materials and methods

2.1 Materials

Myristic acid (MA, $C_{14}H_{28}O_2$, 228.37, white crystal) and 52–54# paraffin wax (PW, white block) were provided by Sinopharm Concoction Reagent Co., Ltd (Shanghai, China). These chemicals were utilized without further depuration.

2.2 Preparation of MA–PW binary mixtures

MA–PW binary mixtures with 20 wt%, 30 wt%, 40 wt%, 50 wt%, 60 wt% and so on wt% of PW were prepared as follows. First of all, MA and PW with a corresponding mass fractions were weighed in a beaker, and sealing them with a film. Secondly, the beaker was put into a water bath magnetic stirrer (DF-101S, Yuhua Co., Ltd, Gongyi, China) with a temperature of 65 °C until the materials were completely melted. Finally, the magnetic stirrer was started to stir for 30 minutes to obtain a uniformly mixed MA–PW binary mixture.

2.3 Cooling curve test

In order to determine the eutectic point of MA–PW binary system, the tubes containing a series of MA–PW binary mixtures were put into a constant temperature water tank (HH-W 600, Changzhou Putian Instrument Manufacturing Co., Ltd) and heated. When the temperature of the samples in the tube reached 65 °C, the test tubes were placed in a constant temperature and humidity incubator (HWS-80B, Tianjin Hongnuo Instrument Co., Ltd) at 10 °C. Moreover, Agilent (34972A) recorded the temperature–time curve of the samples in the process of cooling from 65 °C to 10 °C with a time step of 60 s.

2.4 Thermal properties characterization

DSC (Mettler DSC1) was used to analyze the phase change properties of MA, PW and MA–PW binary eutectic PCM. All tests were conducted in nitrogen atmosphere at a temperature rate of 5 °C min^{-1}. The samples of 5–10 mg were compressed and placed in an aluminum crucible. Then the temperature-heat flow changes of the samples during the process of 20 °C to 65 °C to 20 °C were recorded, and the phase transition temperature and latent heat of the samples were obtained. Furthermore, the thermal stability of MA–PW binary eutectic PCM was checked by TG (Q500, TA Company, USA), and the corresponding experimental conditions were as follows: nitrogen atmosphere, heating rate of 10 K min^{-1}, testing temperature range of 30 °C to 400 °C.

2.5 Accelerated cold–hot cycle test

The MA–PW eutectic PCM was heated from 20 °C to 65 °C in a constant temperature water tank, and then cooled to 20 °C in a constant temperature and humidity incubator, which is a phase change cycle. The accelerated cold–hot cycle test includes 500 phase change cycles. In addition, DSC test was used to evaluate the changes of MA–PW binary PCM after 1, 100, 200 and 500 cycles for phase change properties. Besides, the chemical structure change of MA–PW binary eutectic PCM after 500 cycles was characterized by FT-IR.

2.6 Chemical and crystal characterization

The chemical structure of MA, PW and MA–PW eutectic PCM was characterized by FT-IR (BRUKER TENSOR II, Germany). The scanning band from 600 cm^{-1} to 4000 cm^{-1} and the resolution was 4 cm^{-1}. On the other hand, the crystal structure of MA, PW and MA–PW eutectic PCM was characterized by X-ray diffractometer (PANalytical B.V., Netherlands), using copper target (Kα ray, $\lambda = 1.5406$ Å), diffraction angle from 10° to 80°, step size of 0.01313°, and scan rate was $3^\circ \cdot min^{-1}$.

3. Results and discussion

3.1 Eutectic point of MA–PW binary mixture

The cooling curves of MA, PW and a series of MA–PW binary mixtures with different mass fractions of PW (M_{PW}) are shown in Fig. 1.

As shown in Fig. 1a, the solidification temperatures of MA and PW are 53.4 °C and 50.5 °C, respectively, and the solidification temperature of binary mixtures with any proportion is lower than that of the two pure materials, indicating that the solidification temperature of PCMs can be reduced by the combination of two kinds of PCM. According to the eutectic theory, when the mass fraction of PW is smaller than the eutectic fraction, the solidification temperature of MA–PW binary mixture decreases with the increase of M_{PW}. When the mass fraction of PW is larger than the eutectic fraction, the solidification temperature of MA–PW mixture increases with the increase of M_{PW}. In Fig. 1a, when M_{PW} increases from 30% to 40%, the solidification temperature of MA–PW binary mixture decreases; when M_{PW} increases from 40% to 50%, the solidification temperature of MA–PW binary mixture increases. Moreover, among the MA–PW binary mixtures with M_{PW} of 20%, 30%, 40%, 50%, and 60%, the MA–PW mixture with M_{PW} of 40% has the lowest solidification temperature. Therefore, the eutectic point of the MA–PW binary mixture is considered to be in the range from 30% to 50%, and then the binary mixtures in the range are further analyzed. Fig. 1b presents the cooling curves of the MA–PW binary mixtures with M_{PW} equal to 35%,

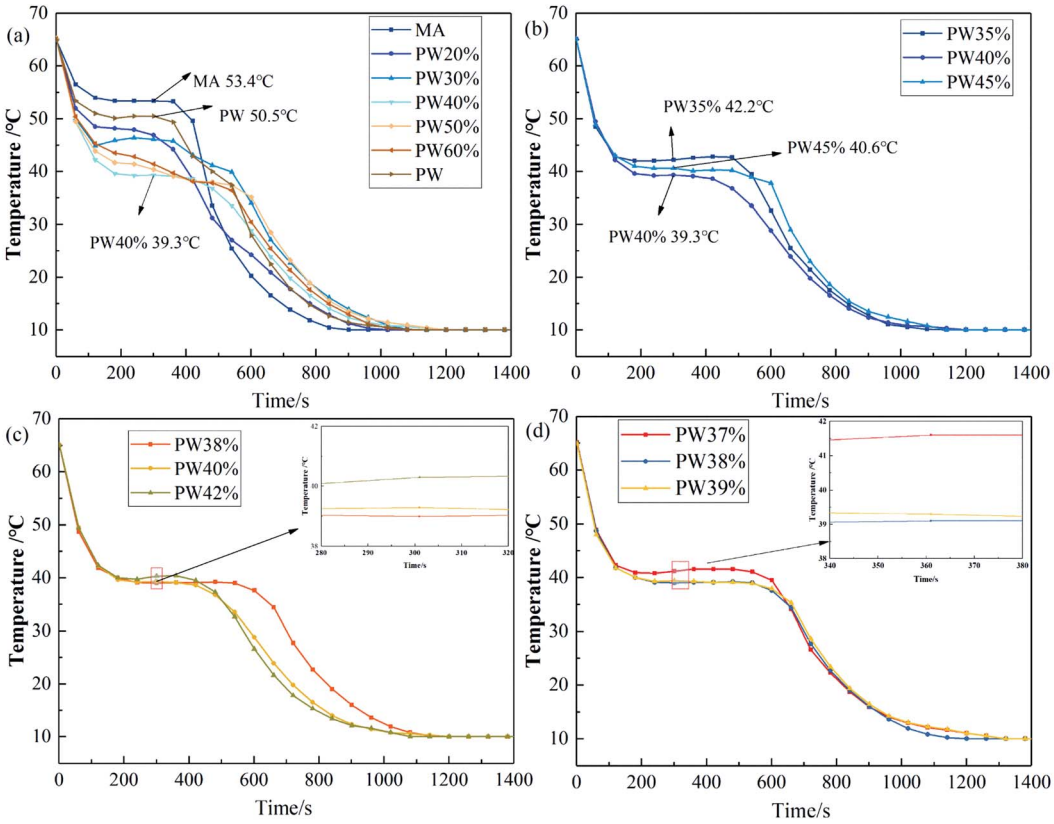

Fig. 1 Cooling curves of (a) MA, PW and MA–PW mixtures of 20–60 wt% PW, (b) MA–PW mixtures of 35 wt% PW, 40 wt% PW and 45 wt% PW, (c) MA–PW mixtures of 38 wt% PW, 40 wt% PW and 42 wt% PW and (d) MA–PW mixtures of 37 wt% PW, 38 wt% PW and 39 wt% PW.

40% and 45%. The solidification temperatures of MA–PW with M_{PW} of 35%, 40% and 45% are found to be 42.2 °C, 39.3 °C and 40.6 °C, respectively. In this range, the solidification temperature of the mixture still showed a trend of first decreasing and then increasing. Therefore, the eutectic point is considered to be in the range from 35% to 45%, and then the binary mixtures in the range are further analyzed. Fig. 1c shows the cooling curves of the MA–PW binary mixtures with M_{PW} equal to 38%, 40% and 42%. The solidification temperatures of MA–PW with M_{PW} of 38%, 40% and 42% are found to be 39.1 °C, 39.3 °C and 39.7 °C, respectively. Obviously, among the MA–PWs with M_{PW} of 38%, 40% and 42%, the MA–PW mixture corresponding to M_{PW} = 38% has the lowest solidification temperature, indicating that the eutectic point is around 38%. Fig. 1d show the cooling curves of the MA–PW binary mixtures with M_{PW} of 37%, 38% and 39%. The solidification temperatures of the binary mixtures with M_{PW} of 37%, 38% and 39% are found to be 41.6 °C, 39.1 °C and 39.2 °C, respectively.

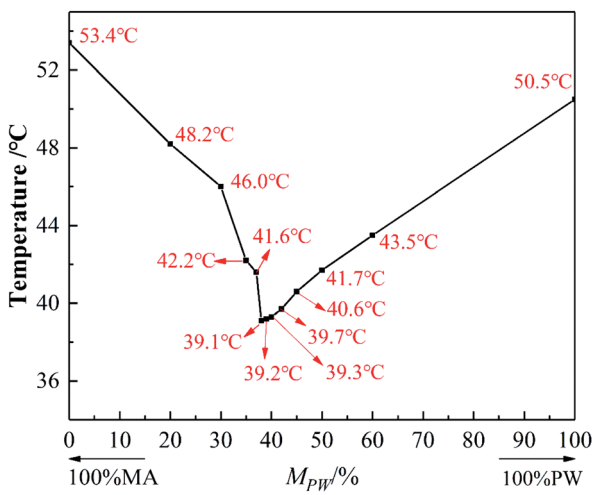

Fig. 2 Solid–liquid phase diagram of MA–PW binary mixtures.

In accordance with the solidification temperature of MA–PW mixtures determined from the cooling curve, the solid–liquid phase diagram of the MA–PW binary mixtures is plotted in Fig. 2 to verify the previous analysis results. It can be seen from Fig. 2 that with the increase of M_{PW}, the solidification temperature of the MA–PW binary mixture shows a trend of first decreasing and then increasing. In addition, the minimum solidification temperature of the binary system corresponds to the mixture with M_{PW} of 38%, its solidification temperature is 39.1 °C. So, the eutectic mass ratio of the MA–PW binary mixture is 62 : 38.

3.2 Phase change properties of MA, PW and MA–PW binary eutectic PCM

The DSC curves of MA, PW and MA–PW binary eutectic PCM are given in Fig. 3, where T_m is the melting temperature, ΔH_m is the

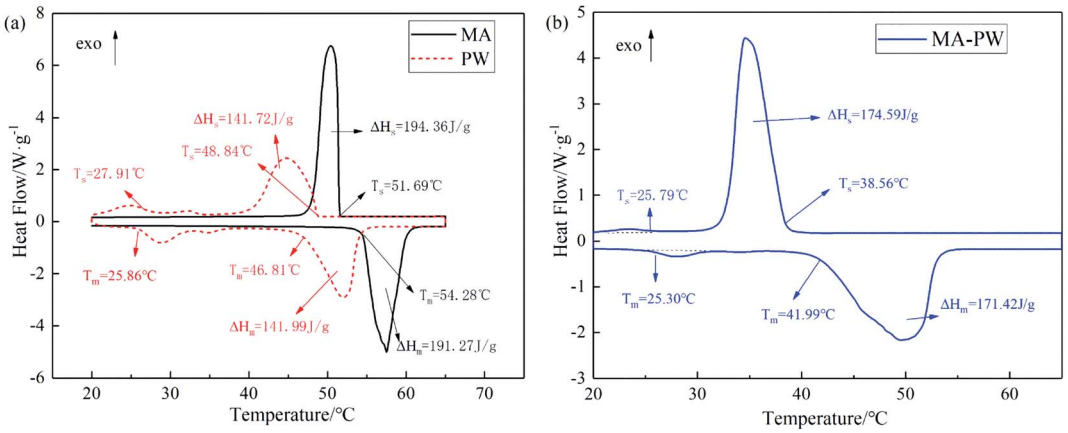

Fig. 3 DSC curves: (a) MA and PW; (b) MA–PW.

latent heat of melting, T_s is the solidification temperature and ΔH_s is the latent heat of solidification (unless otherwise stated, the phase transition temperatures in the paper refer to the extrapolation onset temperature).

From Fig. 3a, it can be found that PW has two kinds of endothermic peaks, a solid–solid phase change peak with low temperature and latent heat, and another solid–liquid phase change peak with melting temperature and latent heat of 46.81 °C and 141.99 J g^{-1}, respectively. In contrast, MA has only one solid–liquid phase change endothermic peak, which corresponds to a melting temperature and latent heat of 54.28 °C and 191.27 J g^{-1}, respectively. Similarly, as shown in Fig. 3b, the MA–PW binary eutectic PCM has two kinds of endothermic peaks, the lower endothermic peak corresponds to a melting temperature of 25.30 °C, and the higher endothermic peak corresponds to a melting temperature and latent heat of 41.99 °C and 171.42 J g^{-1}, respectively.

Comparison of the DSC curves of PW and MA–PW revealed that the onset melting temperatures of their lower endothermic peak were very close, corresponding to 25.86 °C and 25.30 °C, respectively. This phenomenon is attributed to the solid–solid phase transition of PW. Therefore, the lower phase change peak in MA–PW binary eutectic PCM is the solid–solid phase change peaks of PW, and the higher phase change peak is the eutectic peak resulting from the solid–liquid phase change peaks of MA and PW. In addition, the absence of the third peak in the MA–PW binary PCM indicates that the eutectic point was accurately determined.

3.3 Thermal stability of MA–PW binary eutectic PCM

An excellent thermal stability to better handle complex application scenarios. The TG and DTG curves of the MA–PW binary eutectic PCM are given in Fig. 4, and the mass loss of the MA–PW binary eutectic PCM at typical temperatures is listed in Table 1. In this paper, the mass loss of 0.001% was considered as the initial weight loss.

From the TG and DTG curves of MA–PW eutectic PCM, it can be found that MA–PW eutectic PCM decomposed in a single stage, with the started decomposition temperature of 137.86 °C.

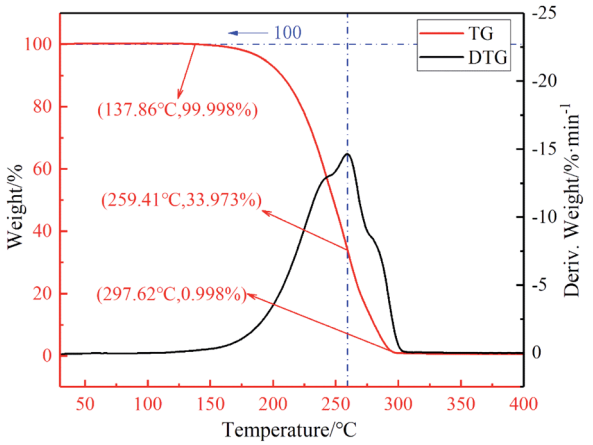

Fig. 4 TG and DTG curves of MA–PW binary eutectic PCM.

Table 1 Mass loss of the MA–PW binary eutectic PCM at typical temperatures

	Temperature/°C				
PCMs	100	150	200	250	300
MA–PW	0	0.315%	7.084%	52.455%	99.100%

The decomposition rate reached the maximum at 259.41 °C, and the material decomposed completely when the temperature reaches 297.62 °C. The application temperature in solar collector field is difficult to reach the decomposition temperature of MA–PW eutectic PCM, which means that MA–PW binary eutectic PCM does not suffer from weight loss such as thermal decomposition in the process of energy storage.

3.4 Chemical structure of MA, PW and MA–PW binary eutectic PCM

The infrared spectra of MA, PW and MA–PW are indicated in Fig. 5.

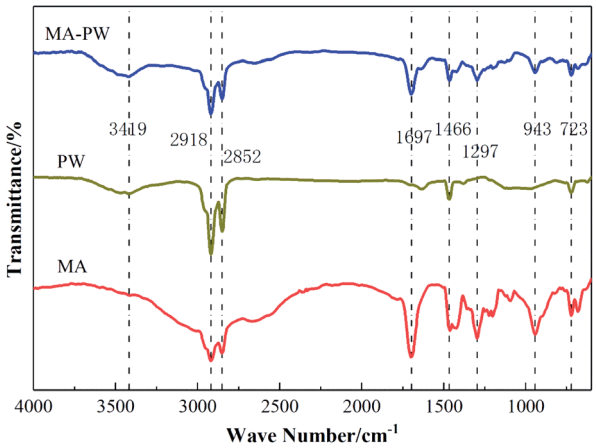

Fig. 5 Infrared spectra of MA, PW and MA–PW.

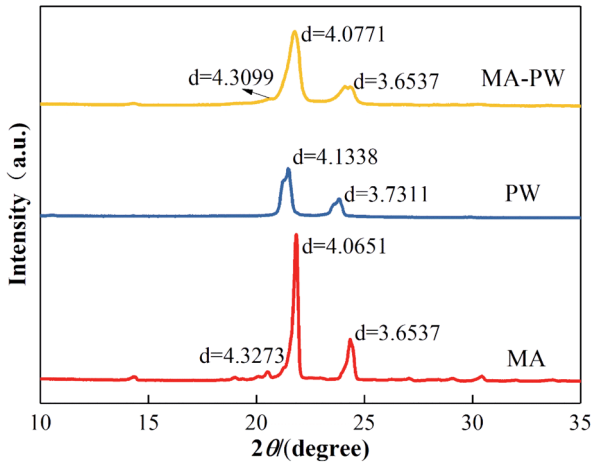

Fig. 6 X-ray diffraction patterns of MA, PW and MA–PW binary eutectic PCM.

According to Fig. 5, firstly, when you look at the FT-IR diagram of MA, you can see that there is a broad absorption peak at 3300 to 2750 cm^{-1} which reflects the stretching vibration of –OH. Moreover, a pair of large peaks appear at 2918 cm^{-1} and 2852 cm^{-1} due to the antisymmetric stretching vibration of $-CH_3$ and symmetric stretching vibration of $-CH_2$, and the characteristic absorption peak for stretch vibrations of C=O is at 1699 cm^{-1}. Besides, the characteristic absorption peak for antisymmetric bending vibrations of $-CH_2$ is at 1462 cm^{-1}, and the in-plane and out-of-plane bending vibration peaks of –OH are located at 1297 cm^{-1} and 943 cm^{-1}, respectively. At last, a peak of absorption is located at 723 cm^{-1} which represents the vibration of the C–H out-of-plane. Secondly, in the FT-IR of PW, there is a characteristic absorption peak at 3419 cm^{-1} due to stretching vibrations of –OH, the absorption peaks appearing at 2918 cm^{-1} and 2852 cm^{-1} are generated by the antisymmetric stretching vibration of $-CH_3$ and the symmetric stretching vibration of $-CH_2$, respectively, the absorption peak at 1468 cm^{-1} is attributed to the antisymmetric bending vibration of $-CH_2$, and the characteristic absorption peak at 723 cm^{-1} is generated by the out-of-plane bending vibration of the C–H bond. Finally, in the FT-IR of MA–PW, different characteristic absorption peaks appear at 3419, 2918, 2852, 1697, 1466, 1297, 943 and 723 cm^{-1}.

Comparing the FT-IR of MA, PW and MA–PW eutectic PCM, we found that the main characteristic absorption peaks of MA–PW eutectic PCM can be found in the absorption peaks of both MA and PW, and the frequency band shift does not exceed 4 cm^{-1}. Moreover, no new characteristic peaks appear in the FT-IR of MA–PW eutectic PCM. The phenomenon indicates that the MA–PW eutectic PCM formed by the mixture of MA and PW was produced by the physical interaction between the components, and no new molecular structure formula was generated by chemical reaction.

3.5 Crystal structure of MA, PW and MA–PW binary eutectic PCM

Fig. 6 shows the XRD patterns of MA, PW and MA–PW binary eutectic PCM, from which it can be found that MA has three diffraction peaks at $2\theta = 20.51°$, $2\theta = 21.85°$ and $2\theta = 24.34°$, corresponding to lattice spacing of 4.3273 Å, 4.0651 Å and 3.6537 Å, respectively, and PW has two diffraction peaks at $2\theta = 21.47°$ and $2\theta = 23.82°$, corresponding to lattice spacing of 4.1338 Å and 3.7311 Å. Similarly, MA–PW shows diffraction peaks at $2\theta = 20.57°$, $2\theta = 21.76°$ and $2\theta = 24.35°$, corresponding to lattice spacings of 4.3099 Å, 4.0771 Å and 3.6537 Å. Therefore, the diffraction peaks of MA–PW binary eutectic PCM are from both with MA and PW, and the maximum angular shift of the diffraction peaks is less than 0.6°. This indicates that MA and PW do not destroy each other's crystal structures after melt blending.

3.6 Reliability of MA–PW binary eutectic PCM

3.6.1 Thermal reliability. Thermal reliability is essential to assess the service life of a material and was determined by comparing the thermal properties of the material before and after accelerated cold–hot cycling experiments. The DSC curves and the corresponding temperature and latent heat of MA–PW binary eutectic PCM after the 1st, 100th, 200th and 500th cycle are given in Fig. 7. As shown in Fig. 7a, the shape and position of the DSC curve of MA–PW remained basically unchanged and no new endothermic and exothermic peaks were generated during 500 cold–hot cycles, which indicates that the MA–PW binary PCM remained a stable eutectic system after 500 cycles. From Fig. 7b and c, it was found that the MA–PW binary eutectic PCM changed by a maximum of 1.45 °C and 7.34 J g^{-1} during 500 cycles for the melting temperature and latent heat of melting, respectively. In addition, its maximum change in solidification temperature and latent heat of solidification were 1.69 °C and 2.09 J g^{-1}, respectively. In conclusion, the maximum relative changes of phase transition temperature and latent heat of MA–PW binary eutectic PCM are less than 5%, and these small changes were completely acceptable in practical applications. Therefore, MA–PW has good thermal reliability and can meet the requirements of engineering applications.

3.6.2 Chemical reliability. In order to evaluate the chemical reliability of the MA–PW eutectic PCM, the MA–PW eutectic

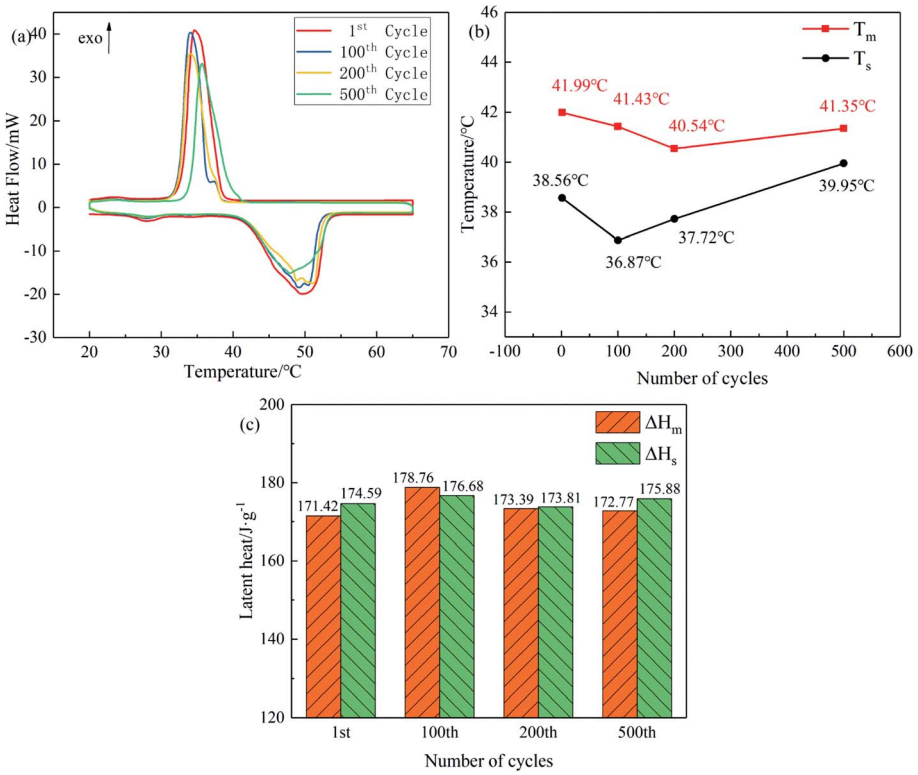

Fig. 7 (a) DSC curves, (b) phase transition temperature and (c) latent heat of MA–PW binary eutectic PCM after 1st, 100th, 200th and 500th cycle.

PCM after the 1st and 500th cycle were analyzed by FT-IR spectroscopy, and the corresponding FT-IR are shown in Fig. 8. Comparing the FI-IR of MA–PW eutectic PCM after 1st and 500th cycle, it is found that the peak shape and absorption bands of the functional groups of the MA–PW binary eutectic PCM did not change during cycling, and no new characteristic absorption peak was generated, which means that the MA–PW binary eutectic PCM has good chemical stability and can meet the durability requirements in practical applications.

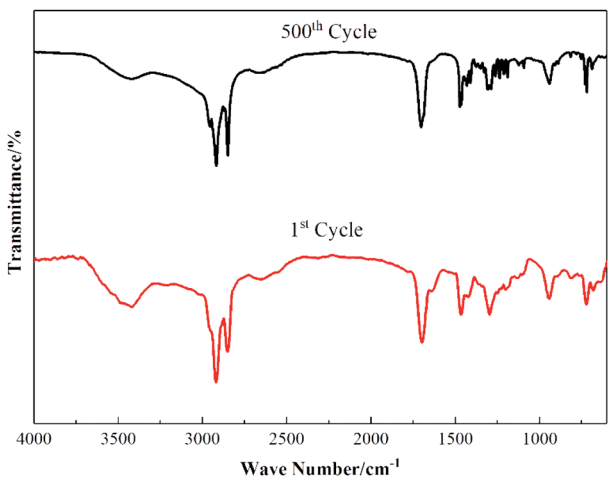

Fig. 8 Infrared spectra of MA–PW after 1st and 500th cycle.

4. Conclusions

A MA–PW binary eutectic PCM was prepared by melt blending method. The thermal properties, chemical structure and crystal structure of the material were analyzed by means of cooling curve, DSC, FT-IR, XRD and TG, and the following conclusions are drawn.

(1) The eutectic point of MA–PW binary system is M_{PW} = 38%, and the corresponding melting temperature and latent heat are 41.99 °C and 171.42 J g^{-1}, respectively.

(2) The thermal decomposition process of MA–PW is a single-stage decomposition. The initial decomposition temperature of 137.86 °C is much higher than the actual application temperature, which indicates that MA–PW has good thermal stability.

(3) During the melt blending process, there is no chemical reaction between MA and PW to generate new molecular structure and no change in crystal structure, which indicates that MA–PW binary eutectic PCM is formed by intermolecular forces.

(4) After 500 cold–hot cycles, the phase transition temperature and latent heat of MA–PW binary eutectic PCM varied less than 5% and its FT-IR did not change significantly, which indicates its excellent reliability and compliance with the requirements of latent heat storage of solar energy.

Conflicts of interest

There are no conflicts to declare.

Acknowledgements

This work was supported by the financial assistance from Jiangxi Province Science and Technology Research Project (GJJ200830) and Jiangxi University of Science and Technology High-level Talents Research Start-up Project (2021205200100553).

References

1 B. Dudley, *BP statistical review of world energy*, BP Statistical Review, London, UK, accessed 6th August, 2018, p. 00116.
2 Y. Zhang, J. Ren, Y. Pu and P. Wang, Solar energy potential assessment: A framework to integrate geographic, technological, and economic indices for a potential analysis, *Renewable Energy*, 2020, **149**, 577–586.
3 J. P. Da Cunha and P. Eames, Thermal energy storage for low and medium temperature applications using phase change materials–a review, *Appl. Energy*, 2016, **177**, 227–238.
4 S. Zhang, W. Wu and S. Wang, Experimental investigations of alum/expanded graphite composite phase change material for thermal energy storage and its compatibility with metals, *Energy*, 2018, **161**, 508–516.
5 B. Nghana and F. Tariku, Phase change material's (PCM) impacts on the energy performance and thermal comfort of buildings in a mild climate, *Build. Sci.*, 2016, **99**, 221–238.
6 L. Xia and P. Zhang, Thermal property measurement and heat transfer analysis of acetamide and acetamide/expanded graphite composite phase change material for solar heat storage, *Sol. Energy Mater. Sol. Cells*, 2011, **95**(8), 2246–2254.
7 X. Huang, X. Chen, A. Li, D. Atinafu, H. Gao, W. Dong and G. Wang, Shape-stabilized phase change materials based on porous supports for thermal energy storage applications, *Chem. Eng. J.*, 2019, **356**, 641–661.
8 Y. Zhang, J. Wang, J. Qiu, X. Jin, M. M. Umair, R. Lu and B. Tang, Ag-graphene/PEG composite phase change materials for enhancing solar-thermal energy conversion and storage capacity, *Appl. Energy*, 2019, **237**, 83–90.
9 S. Kahwaji, M. B. Johnson, A. C. Kheirabadi, D. Groulx and M. A. White, A comprehensive study of properties of paraffin phase change materials for solar thermal energy storage and thermal management applications, *Energy*, 2018, **162**, 1169–1182.
10 B. Mu and M. Li, Synthesis of novel form-stable composite phase change materials with modified graphene aerogel for solar energy conversion and storage, *Sol. Energy Mater. Sol. Cells*, 2019, **191**, 466–475.
11 X. Huang, Y. Lin, G. Alva and G. Fang, Thermal properties and thermal conductivity enhancement of composite phase change materials using myristyl alcohol/metal foam for solar thermal storage, *Sol. Energy Mater. Sol. Cells*, 2017, **170**, 68–76.
12 D. Rozanna, T. G. Chuah, A. Salmiah, T. S. Choong and M. Sa'Ari, Fatty acids as phase change materials (PCMs) for thermal energy storage: a review, *Int. J. Green Energy*, 2005, **1**(4), 495–513.
13 R. K. Sharma, P. Ganesan, V. V. Tyagi, H. S. C. Metselaar and S. C. Sandaran, Developments in organic solid–liquid phase change materials and their applications in thermal energy storage, *Energy Convers. Manage.*, 2015, **95**, 193–228.
14 A. Sharma and A. Shukla, Thermal cycle test of binary mixtures of some fatty acids as phase change materials for building applications, *Energy Build.*, 2015, **99**, 196–203.
15 S. Kahwaji, M. B. Johnson, A. C. Kheirabadi, D. Groulx and M. A. White, Fatty acids and related phase change materials for reliable thermal energy storage at moderate temperatures, *Sol. Energy Mater. Sol. Cells*, 2017, **167**, 109–120.
16 M. Pan and W. Lai, Cutting copper fiber/paraffin composite phase change material discharging experimental study based on heat dissipation capability of Li-ion battery, *Renewable Energy*, 2017, **114**, 408–422.
17 L. Xia, P. Zhang and R. Z. Wang, Preparation and thermal characterization of expanded graphite/paraffin composite phase change material, *Carbon*, 2010, **48**(9), 2538–2548.
18 G. Zhao, X. Xu, L. Qiu, X. Zheng and D. Tang, Study on the heat conduction of phase-change material microcaPWules, *J. Therm. Sci.*, 2013, **22**(3), 257–260.
19 H. Ke, Z. Pang, B. Peng, J. Wang, Y. Cai, F. Huang and Q. Wei, Thermal energy storage and retrieval properties of form-stable phase change nanofibrous mats based on ternary fatty acid eutectics/polyacrylonitrile composite by magnetron sputtering of silver, *J. Therm. Anal. Calorim.*, 2016, **123**(2), 1293–1307.
20 C. Liu, Y. P. Yuan, N. Zhang, X. L. Cao and X. J. Yang, Theoretic prediction of phase change temperature and latent heat of fatty acids ternary eutectic mixture, *Mater. Rev.*, 2014, **28**(1), 165–168.
21 A. Karaipekli, A. Sari and K. A. M. İ. L. Kaygusuz, Thermal properties and long-term reliability of capric acid/lauric acid and capric acid/myristic acid mixtures for thermal energy storage, *Energy Sources, Part A*, 2008, **30**(13), 1248–1258.
22 A. Karaıpeklı, A. Sarı and K. Kaygusuz, Thermal properties and thermal reliability of capric acid/stearic acid mixture for latent heat thermal energy storage, *Energy Sources, Part A*, 2009, **31**(3), 199–207.
23 V. Chinnasamy and S. Appukuttan, Preparation and thermal properties of lauric acid/myristyl alcohol as a novel binary eutectic phase change material for indoor thermal comfort, *Energy Storage*, 2019, **1**(5), e80.
24 G. Ma, S. Liu, S. Xie, Y. Jing, Q. Zhang, J. Sun and Y. Jia, Binary eutectic mixtures of stearic acid-n-butyramide/n-octanamide as phase change materials for low temperature solar heat storage, *Appl. Therm. Eng.*, 2017, **111**, 1052–1059.